Spectroscopy of the hydrogen 1*S*-3*S* transition with chirped laser pulses

D. C. Yost,[1,*] A. Matveev,[1] A. Grinin,[1] E. Peters,[1] L. Maisenbacher,[1] A. Beyer,[1] R. Pohl,[1]
N. Kolachevsky,[2,3] K. Khabarova,[2,3] T. W. Hänsch,[1,4] and Th. Udem[1]

[1]*Max-Planck-Institut für Quantenoptik, 85748 Garching, Germany*

[2]*P. N. Lebedev Physics Institute, 119991 Moscow, Russia*

[3]*Russian Quantum Center, 143025 Skolkovo, Russia*

[4]*Ludwig-Maximilians-Universität, München, Fakultät für Physik, Schellingstrasse 4/III, 80799 München, Germany*

(Received 28 September 2015; revised manuscript received 1 March 2016; published 20 April 2016)

We identify a systematic present in two-photon direct frequency comb spectroscopy (DFCS) which is a result of chirped laser pulses and is a manifestation of the first-order Doppler effect. We carefully analyze this systematic and propose methods for its mitigation within the context of our measurement of the hydrogen 1*S*-3*S* transition. We also report on our determination of the absolute frequency of this transition, which is comparable to a previous measurement using continuous-wave spectroscopy [O. Arnoult *et al.*, Eur. Phys. J. D **60**, 243 (2010)], but was obtained with a different experimental method.

DOI: 10.1103/PhysRevA.93.042509

I. INTRODUCTION

Hydrogen is the simplest stable atom and, as such, its energy levels can be calculated with high precision [1]. Its study is of fundamental importance in modern physics and has been instrumental in the development of quantum mechanics and quantum electrodynamics (QED). Currently, hydrogen spectroscopy remains a stringent test of QED, and, with the persisting discrepancies in the determinations of the proton charge radius through comparisons of muonic hydrogen and normal hydrogen [1–4], is not devoid of modern controversy.

While hydrogen is a near ideal system for testing bound-state QED, there are two parameters which limit the theoretical determination of its energy levels: the Rydberg constant and the rms proton charge radius. However, by measuring several transitions in hydrogen which depend differently on these input parameters, the Rydberg constant and proton size can be extracted [1,5,6]. The consistency of these measurements is then effectively a test of QED. In addition, the proton size has been determined with an experiment which is intrinsically more sensitive: the measurement of the 2*S*-2*P* Lamb shift in muonic hydrogen mentioned above [2,3]. Mysteriously, these two determinations of the proton radius disagree by 4 combined standard deviations [4]. The CODATA value for the proton charge radius takes into account both regular hydrogen spectroscopy and electron-proton scattering measurements and disagrees with the muonic hydrogen value by 7 combined standard deviations [1]. Therefore, studies of muonic hydrogen, rather than removing a burden from the hydrogen spectroscopist, have provided a strong motivation for further study and new experimental techniques.

In an attempt to produce experimental data relevant to the proton radius puzzle, we have, along with the Biraben group in Paris, pursued spectroscopy of the 1*S*-3*S* transition of atomic hydrogen [7–9]. This transition is a good choice for precision measurement because it is a ground-state transition with a relatively narrow natural linewidth of only 1 MHz and, being a two-photon transition, is well suited to Doppler-free spectroscopy. One disadvantage is that the excitation requires 205-nm radiation, which is difficult to produce in readily available nonlinear crystals. To increase the harmonic efficiency, we use a pulsed laser with ∼2-ps pulse length. In the frequency domain, this can be described as a comb of frequency modes which can still be used for high-precision spectroscopy. However, the frequency conversion steps necessary to produce the 205-nm radiation proceed more easily than with a continuous-wave (cw) source due to the higher peak power of the pulsed source. Further, this measurement is an implementation of direct frequency comb spectroscopy (DFCS) in precision hydrogen spectroscopy.

The use of pulsed lasers for precision spectroscopy has recently gained attention since many transitions of simple atomic and ionic systems lie in difficult-to-reach spectral regions. Pulsed lasers, combined with frequency comb techniques (where the pulse-to-pulse coherence is utilized), offer efficient nonlinear conversion, broad spectral coverage, and seemingly limitless coherence times [10–14]. While 205-nm radiation can be produced in the cw regime [15], the spectroscopy of hydrogenlike ions will require wavelengths in the VUV and XUV which will, by any reasonable forecast, require pulsed radiation sources [13]. Therefore, we also consider this experiment to be an excellent testing ground for precision measurement using DFCS.

At first glance, one would expect two-photon DFCS using counterpropagating laser pulse trains to be free from first-order Doppler shifts—much like two-photon spectroscopy using cw lasers. As discussed in [16], two-photon DFCS can be understood by considering the pairwise addition of modes from two counterpropagating frequency combs. All pairs of comb modes whose frequencies add to the transition frequency will coherently contribute to the excitation. The first-order Doppler cancellation will not be perfect for two comb modes of unequal frequencies. However, for every pair of modes which would produce a positive frequency shift, there is a counterpart pair of modes producing a negative shift such that a broadening of the line but no systematic shift results [16]. Pulse chirp does not shift the frequency of the individual comb modes

*Present address: Department of Physics, Colorado State University, Fort Collins, Colorado 80523, USA; Corresponding author: dylan.yost@colostate.edu

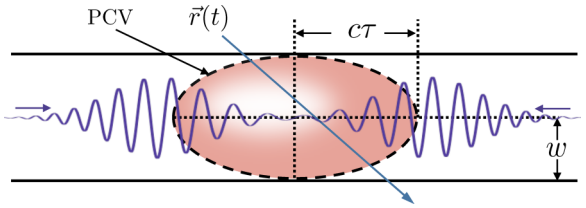

FIG. 1. Diagram showing the pulse collision volume (PCV) resulting from colliding pulse trains (frequency combs). Also shown in the diagram are the lengths w and $c\tau$ along with a representative atomic trajectory $\vec{r}(t)$.

but only affects their relative phases, which may lead one to assume that the pulse chirp would not produce any systematic effects. However, the chirp also creates a spatial variation of the phase along the direction of laser propagation that, when coupled with the motion of the atoms, can lead to a systematic effect which we term the chirp-induced first-order Doppler shift (CIFODS). It is this effect that is the focus of this article.

We believe that DFCS will become an increasingly important technique for future spectroscopy of simple atoms and, therefore, we discuss possible routes for the further mitigation of this systematic. This discussion is also timely considering that several authors have recently discussed DFCS with chirped pulses so that a Doppler-broadened background can be suppressed [17,18].

II. THEORETICAL DESCRIPTION OF THE CHIRP-INDUCED FIRST-ORDER DOPPLER SHIFT

Our experiment is performed with two counterpropagating trains of pulses (frequency combs). We describe the pulse trains traveling in the positive and negative z directions by

$$\mathcal{E}_{\pm} = A_0 \sum_n e^{-(1+ib)(t-nt_r \pm z/c)^2/\tau^2 - \rho^2/w^2 - i\omega_c t \mp i k_c z}, \quad (1)$$

where t_r is the repetition period, τ is the pulse length, ω_c is the carrier frequency, $k_c = \omega_c/c$, ρ is the radial position, z is the position along the direction of beam propagation, and w is the radial width of the laser beam (assumed to be cylindrically symmetric). This form is valid in the weak-focusing (plane-wave) approximation. We include possible chirp of the pulses with the parameter b—note that the sign of b does not change upon backreflection that reverses the propagation direction. The Doppler-free two-photon signal will occur only at the position where the pulses collide (see Fig. 1), and the two-photon Rabi frequency [19] will be proportional to the product of the counterpropagating pulse trains given by

$$\mathcal{E}_+\mathcal{E}_- = A_0^2 \sum_n e^{-2(1+ib)[(t-nt_r)^2+z^2/c^2]/\tau^2 - 2\rho^2/w^2 - 2i\omega_c t}. \quad (2)$$

We consider only the pulse collision volume near $z \approx 0$, where we assume there is significant atom density. To take into account the motion of the atoms in the z direction, we let $z(t) = z_0 + v_z t$. If we ignore the second-order Doppler shift, this leads to an instantaneous frequency shift in the reference frame of the atom of

$$\frac{d}{dt}\left(-b\frac{2z^2(t)}{c^2\tau^2}\right) \to -b\frac{4v_z z(t)}{c^2\tau^2}. \quad (3)$$

We do not take into account the phase shift in Eq. (2) given by $-2b(t-nt_r)^2/\tau^2$, because it is identical for every pulse and therefore does not shift the position of the comb modes [16]. The frequency shift shown in Eq. (3) is an odd function of both the position, $z(t)$, and the velocity, v_z, where $z = 0$ is defined as the center of the pulse collision volume. Therefore, in a gas cell, where there is no preferential direction of atomic motion, we expect that there are no systematic frequency shifts from this effect due to symmetry. The shifts from individual atomic trajectories would instead lead to a broadening of the measured line. In an experiment utilizing a divergent atomic beam, the situation is more complicated because the symmetry is, in general, broken.

To gain additional insight into this problem, we consider an atom in a well-defined trajectory, $r(t) = (x_0 + v_x t, y_0 + v_y t, z_0 + v_z t)$, as shown in Fig. 1. We then perform the Fourier transform of Eq. (2). The overall expression is lengthy but the result is a comb of frequencies centered about $2\omega_c$ and spaced by $f_r = 1/t_r$. The individual comb modes are broadened due to the finite interaction time as the atom traverses the pulse collision volume. In addition, the comb modes are shifted in frequency due to the CIFODS. This shift can be extracted and is given by

$$\delta\omega = b\frac{4v_z\left(v_x v_z x_0 + v_y v_z y_0 - \left(v_x^2 + v_y^2\right)z_0\right)}{v_z^2 w^2 + \left(v_x^2 + v_y^2\right)c^2\tau^2}. \quad (4)$$

In contrast to Eq. (3), this expression takes into account the total flight of the atom across the pulse collision volume. From this we see that the existence of a systematic shift requires that b, v_z and either v_x or v_y must all be nonzero.

Equation (4) can be distilled into more manageable expressions by examining representative trajectories. First, we consider an atom which travels predominantly along the propagation direction of the laser beam such that

$$\vec{r}(t) = (v_x t + x_0, 0, v_z t), \quad (5)$$

where we assume that $v_z \gg v_x$. Although we have set v_y and y_0 to zero, the problem is cylindrically symmetric about the z axis so that this will result in a general expression. In addition, we can set $z_0 = 0$ because the choice of $t = 0$ is arbitrary and assume that the lengths $c\tau$ and w are of the same order of magnitude. In this case, the shift given by Eq. (4) is approximately

$$\delta\omega \approx b\frac{4v_x x_0}{w^2}. \quad (6)$$

As a second representative case, we consider an atomic trajectory where the atom is moving transverse to the laser beam such that

$$\vec{r}(t) = (v_x t, v_y t + y_0, v_z t + z_0), \quad (7)$$

where now $v_x \gg v_y, v_z$ and we have set $x_0 = 0$ by choosing an appropriate $t = 0$. In that case the shift is

$$\delta\omega \approx -b\frac{4v_z z_0}{c^2\tau^2}. \quad (8)$$

Equations (6) and (8) are similar except that in Eq. (8), the length of the pulse collision volume $c\tau$ functions as the beam

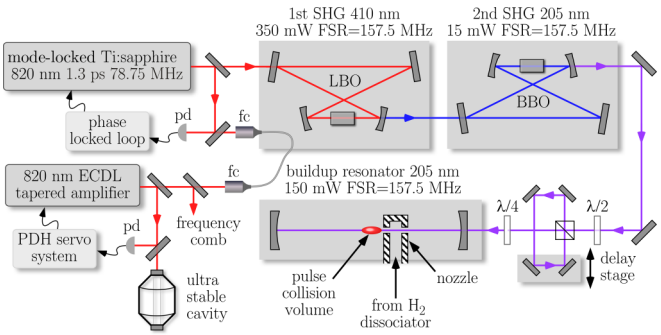

FIG. 2. Experimental setup: A mode-locked 820-nm Ti:sapphire laser is frequency quadrupled to 205 nm using two resonant doubling stages. This radiation is then sent to an enhancement cavity where spectroscopy of atomic hydrogen is performed. A delay stage external to the spectroscopy cavity is used to create counterpropagating pulses inside the cavity. pd: photodiode, fc: fiber coupler, $\lambda/4$: quarter-wave plate, $\lambda/2$: half-wave plate.

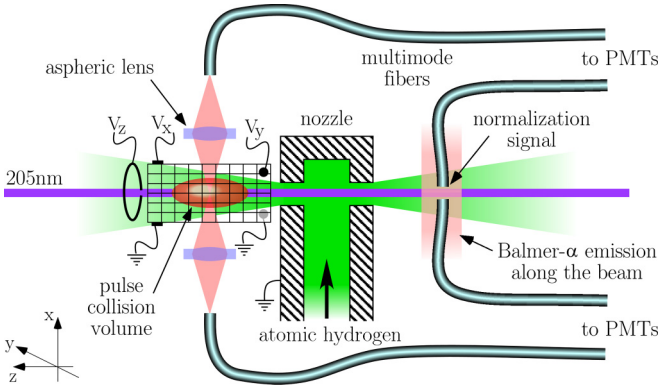

FIG. 3. Hydrogen nozzle and detector. Atomic hydrogen enters the nozzle and exits along the laser beam path. Four aspheric lenses (only two are shown in the figure) with focal lengths of 2.76 mm focus the fluorescence onto multimode optical fibers (1-mm-diameter core, 0.48 NA). Copper grids coated in colloidal graphite surround the pulse collision volume on four sides. By controlling the voltage on two of these grids (V_x and V_y) along with the voltage applied to a wire ring (V_z), we can adjust the electric field at the pulse collision volume. Four multimode fibers also collect fluorescence on the back side of the nozzle. In that location—away from the pulse collision volume—only the Doppler-broadened signal is present, which is used for normalization. This normalization is required due to fluctuating laser power and atom density. Because there is no need to prevent dc stark shifts on the normalization signal, we forego the electrodes.

radius w. In our case, these two lengths are of the same order of magnitude and there is not a great advantage in one experimental geometry over the other.

The expression given by Eq. (4) along with the approximate expressions given by Eqs. (6) and (8) reveal effective strategies for minimizing the chirp-induced systematic. Some obvious choices are to minimize the pulse chirp or the velocity of the atomic beam. However, Eq. (4) also indicates that increasing the time of flight through the pulse collision volume (by increasing w and $c\tau$) would also reduce the effect. If we are in a regime where we can apply the approximations given by Eq. (6), then the use of highly collimated atomic beams traveling along the z axis could also be an effective strategy. Similarly, for an atomic beam traveling normal to the laser beam, Eq. (8) is applicable and indicates that increased collimation of the atomic beam, which in this case corresponds to a decrease in v_z, would mitigate the systematic.

Equation (4) and the following discussion treats only a single atomic trajectory. In many cases, one can simply average this equation over the ensemble of atomic trajectories with no great difficulty. However, in our current experimental setup, our detector collects fluorescence from an area only 800 μm in diameter whereas $c\tau \approx 500$ μm. The detector is therefore small enough that we will not necessarily collect the fluorescence from each trajectory with equal probability. Instead, we will sample a different ensemble of atomic trajectories depending on its position. Due to this added complication, it is more effective to analyze our experiment using a numerical integration of the optical Bloch equations, as discussed in Sec. IV. The small detector we are currently using is ideal for the study of the chirp-induced systematic. However, we believe that, for suppression of this systematic, a larger detector will be beneficial as it will lead to a more even sampling of the atomic trajectories and allow us to use Eq. (4) and the approximations resulting from it.

III. EXPERIMENTAL SETUP

Our experimental setup is shown in Fig. 2 and is similar to our previous experiment described in [8]. We produce a frequency comb at 205 nm by frequency quadrupling an 820-nm, ~2-ps pulse length Ti:sapphire laser. We determine the absolute frequency of the 820-nm laser by locking a single comb mode to a cw external cavity diode laser (ECDL) also at 820 nm. The ECDL is itself locked to an ultrastable cavity and its frequency is measured with a self-referenced frequency comb. With this referencing scheme and by measuring the repetition frequency of the ~2-ps Ti:sapphire laser, the comb mode positions of that laser are fully determined.

The frequency quadrupling takes place in two enhancement cavities. The first utilizes a lithium triborate (LBO) nonlinear crystal and the second, beta barium borate (BBO) crystal. The laser produces a 78.8-MHz pulse train, but the first doubling cavity also acts as a mode filtering cavity so that we obtain a frequency comb with a 157.5-MHz repetition rate at 410 nm and an average power of ~350 mW. After the second doubling cavity, we obtain ~15 mW of 205-nm radiation, which is sent to an enhancement cavity with a power buildup of ~10 for spectroscopy. The mirrors of the enhancement cavity have a radius of curvature of 500 mm, which produces a beam radius of 90 μm at the center of the cavity. Before the enhancement cavity, a polarization-dependent delay stage is set to within 60 fs of exactly half the repetition period of the frequency comb. This produces two pulses which collide with each other twice every repetition period at the center of the cavity. We use a quarter-wave plate before the cavity so that the two counterpropagating pulses have σ_+ and σ_- polarizations, respectively. This reduces the excitation of the $1S-3D$ transitions with respect to the $1S$-$3S$ transitions [20] (see Fig. 5). The enhanced 205-nm radiation travels through an aluminum nozzle, as shown in Fig. 3, which we use to inject atomic hydrogen along the laser beam path.

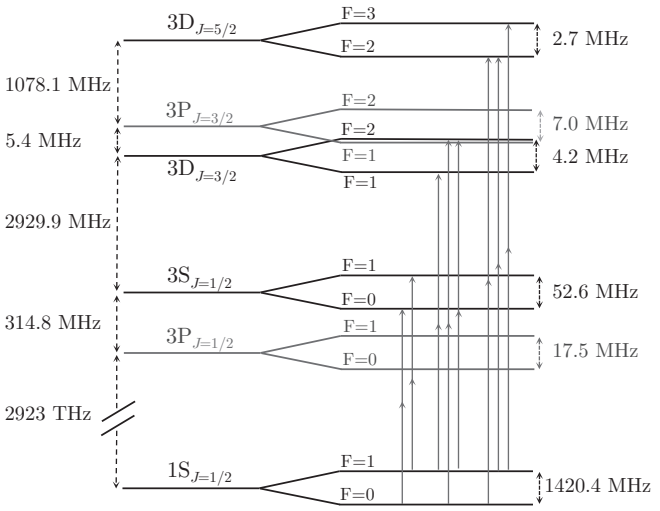

FIG. 4. Diagram showing the relevant levels and two-photon transitions in hydrogen. The hyperfine splitting of the $3D$ states is unresolved due to the 10.3-MHz natural linewidth of the $3D$ states. The $3P_{3/2}$ and $3D_{3/2}$ states are easily mixed with electric fields due to their small energy difference.

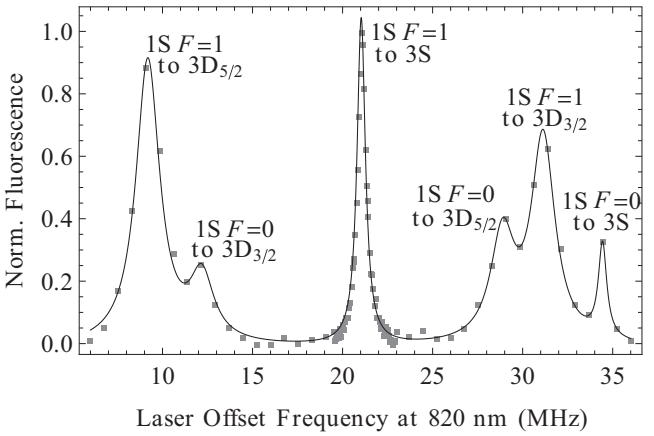

FIG. 5. Experimental fluorescence signal as the frequency offset between one frequency comb mode of the Ti:sapphire laser and the stabilized ECDL is scanned. (The solid line represents Lorentzian fits for the individual lines.) The F quantum number labels correspond to the $1S$ state. For the transitions to the $3S$ states, only $\Delta F = 0$ transitions are allowed. The repetition rate of the laser was chosen so that the $1S$-$3S$ $F = 1$ transition is well isolated.

After excitation to the $3S$ or $3D$ states, the atoms decay to the $2P$ state, emitting a 656-nm photon. Our detection scheme is shown in Fig. 3. As can be seen from the figure, we collect fluorescence from two locations—the pulse collision volume and also on the other side of the hydrogen nozzle, roughly 2 cm away from the pulse collision volume. From the pulse collision volume, we obtain signal where the first-order Doppler broadening is greatly suppressed. At the other location, only a Doppler-broadened signal is present and the lines are broadened to ∼20 GHz. The comb spacing is only 157.5 MHz so that there is no dependence of the fluorescence signal on the offset frequency of the frequency comb from the Doppler-broadened signal. However, this signal provides us with important information, since all fluctuations of the two-photon signal due to atom number and laser power will be present. We do a point-by-point normalization of our data using the Doppler-broadened signal, which removes a large amount of the technical noise.

The bandwidth of the frequency comb is ∼200 GHz, whereas the splitting between the $3S$ and $3D$ transitions is ∼3 GHz (see Fig. 4) so that as the offset between the 820-nm frequency comb and the ECDL is scanned, all two-photon allowed transitions from the $1S$ state to the $3S$ and $3D$ states are observed. When frequency doubling a frequency comb, the offset frequency of the frequency comb is also doubled whereas the repetition rate is not. Therefore to scan the offset frequency of the 205-nm comb by one repetition rate (157.5 MHz after the mode filtering of the first doubling stage) requires that we scan the offset of the comb at 820 nm by only 39.4 MHz. As a result, all two-photon allowed transitions are observed in this relatively small scan range. This behavior is shown in Fig. 5.

The pattern shown in Fig. 5 is highly dependent on the repetition rate of the frequency comb. The repetition rate of 157.5 MHz was chosen so that the $1S$ $F = 1$ to $3S$ $F = 1$ transition would be relatively isolated and, thus, well-suited for precision measurement. That being said, the whole structure shown in Fig. 5 is, in principle, usable for absolute frequency determinations—albeit the modeling of the structure is very involved. We also found that the relative heights of the transitions gave sensitive information on stray electric fields. This is because the $3D_{3/2}$ state is nearly degenerate with the $3P_{3/2}$ state and therefore very easily quenched with an electric field [21]. A reduction of the fluorescence signal from the $3D_{3/2}$ state relative to the $3D_{5/2}$ indicated that stray electric fields were present at the interaction volume.

We use room temperature hydrogen so that the average speed of the atoms leaving the nozzle is ∼2700 m/s. The pulse collision volume is only ∼500 μm long and 180 μm in diameter so that the measured transitions are transit-time broadened to ∼4.5 MHz. Also, the pulse collision volume is reimaged in such a way that the effective diameter of the detection region is only 800 μm. In this way we can preferentially detect the fluorescence coming from atoms at different points in their trajectories by adjusting the relative position of the detector and pulse collision volume.

IV. RESULTS AND DISCUSSION

Measurements of the absolute frequency as a function of detector position were performed on five separate days and are shown in Fig. 6. There is a near linear relationship between the measured transition frequency and the detector position. The position $z = 0$ is defined as the center of the pulse collision volume and is determined experimentally through measurements of the on-resonance signal strength as a function of position along the z axis. The slopes of these curves correspond to the pulse chirp and depend on the measurement day. We believe this day-to-day variation is due to alignment changes of the laser and/or doubling and quadrupling stages.

We also simulated our experimental results through numerical integration of the optical Bloch equations. We performed the integration over the atomic trajectories and

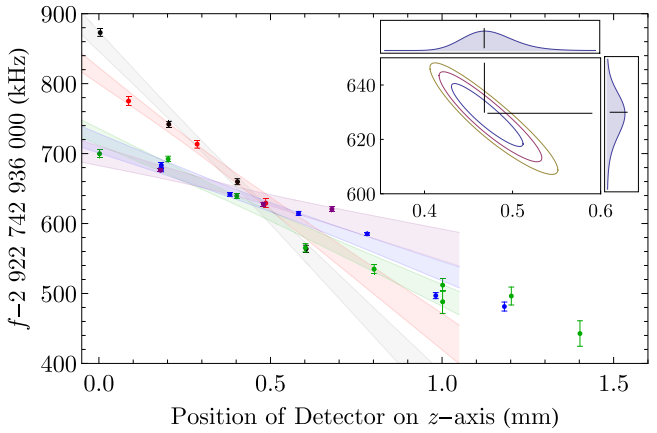

FIG. 6. Measured frequency f of the observed $1S$-$3S$ $F = 1$ line center as a function of detector position. The observed resonance was determined by fitting the experimental data with a Lorentzian line shape. Data points of a certain color were all taken on the same day and the change in slope from day to day is due to a variation of the pulse chirp b. From our simulations, the observed slopes correspond to a variation of b from ∼0.15 to ∼0.7. The wide stripes represent pointwise 68% confidence bands for a simple linear regression analysis of 1 day of data. The crossing of these confidence bands gives a confidence region for the experimental coordinates of the crossing point on the (z, f) plane. The 68%, 95%, and 99.7% confidence regions for this point are shown on the upper-right plot, together with projections of the resulting likelihood function on the z and f axes. Data points at large detector misalignment (>1 mm) lie in a region where we do not expect a linear variation with detector position and so these data points are excluded in the data analysis.

velocities through both a Monte Carlo method and by direct Gaussian quadrature. The angles of the trajectories with the beam axis are assumed to follow a cosine distribution for each point of the nozzle orifice. The results for the Monte Carlo method are shown in Fig. 7. We see from the simulations that

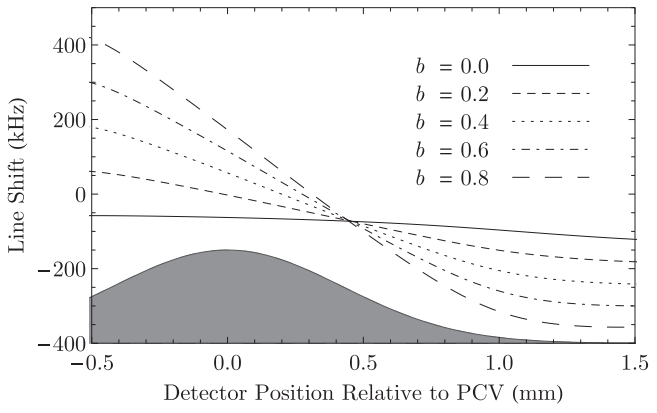

FIG. 7. Simulated frequency shifts using the Monte Carlo method for different values of the chirp parameter b as a function of detector offset from the center of the pulse collision volume (PCV). In addition to the CIFODS, the simulations include the second-order Doppler shift. The gray shaded region shows the relative position and size of the pulse collision volume. The position where the curves intersect is insensitive to the chirp parameter b, and the remaining frequency shift is due to the second-order Doppler effect.

within a certain region near the pulse collision volume, there is also a linear relationship between the transition frequency and the detector position due to the CIFODS—this is in qualitative agreement with our experimental results and is motivated physically by Eq. (3).

As can be seen in Figs. 6 and 7, the curves for different b values approximately cross at one point on the (z, f) plane where f is the center of the observed resonance determined by a least-squares fitting procedure. At this point, the signal from the atomic beam is sampled in such a way that the CIFODS is minimized. To extract the position of the experimental crossing point and its uncertainty we made two assumptions. The first is that the chirp of the laser pulses does not vary significantly during the measurement day. Second, if b is fixed, then the function $f(z,b)$ is assumed to be linear in z so that $f(z) = \alpha z + \beta$. This assumption is supported both by the data and by simulations. For every measurement day i we found a two-dimensional likelihood function $\xi_i(z, f)$ of the position of the $f(z)$ on (z, f) plane using a linear regression routine. (See the corresponding confidence bands in Fig. 6.) The product of the likelihood functions $\xi(z, f) = \prod \xi_i(z, f)$ obtained for different days gives a likelihood function of the crossing point position on the (z, f) plane. The maximum of the final $\xi(z, f)$ function is at the point $z_{cross} = 0.47(3)$ mm, and $f_{cross} =$ 2 922 742 936 629.6(8.4) kHz. The simulations show that the chirp is almost perfectly compensated at $z_{cross} = 0.45(13)$ mm, which is in good agreement with the experimental results. Moreover, the two simulations (Monte Carlo and direct Gaussian quadrature) produce the same value for f_{cross} to within 3 kHz. It may seem surprising that the intersection point shown in Figs. 6 and 7 is away from the center of the pulse collision volume. However, the atoms are traveling predominantly along the z axis and the lifetime of the $3S$ state is long enough (∼160 ns) that the position of maximum fluorescence is offset significantly from the center of the pulse collision volume as well. Therefore, offsetting the detector slightly in the positive z direction actually results in a more even sampling of the fluorescence from the different atomic trajectories.

The simulated results in Fig. 7 assume that the pulse chirp is quadratic, as defined in Eq. (1). However, it is probable that the chirp is due to to self-phase modulation (SPM) in the nonlinear crystals. This would impose a phase shift on an individual pulse that is proportional to $n_2\, e^{-2(t\pm z/c)^2/\tau^2}$, where n_2 is the nonlinear index of refraction. While the leading term in this phase shift will still result in a quadratic chirp (ignoring an unimportant constant phase shift), it was not possible to give a closed-form expression for the CIFODS as in Eq. (4) using the full expression. To investigate the effects of SPM further, we also simulated the experiment assuming the chirp arises from SPM and we found in this case, $z_{cross} = 0.485(10)$ mm and f_{cross} is within 200 Hz of the previous result. However, at detector positions far away from z_{cross}, the simulations assuming the chirp arises from SPM do not agree with the simulations assuming quadratic pulse chirp and both show nonlinear behavior. For this reason, we do not include the experimental data points within this region in our data analysis.

With the experimentally determined value of f_{cross}, we are able to make an absolute frequency determination of the $1S$-$3S$ transition because this value is, by definition, insensitive to the

TABLE I. Corrections and uncertainties (Δf) for the hydrogen $1S$-$3S$ determination (kHz).

Item	Frequency/correction	Δf
Crossing point	2 922 742 936 629.6	8.4
Second-order Doppler	+73	13
Pressure shift	+10.3	6.3
DC Stark effect	0	1.7
AC Stark effect	–0.4	0.2
Zeeman effect	0	0.005
Line pulling [22]	–2.0	1.0
Total $f_{1S\text{-}3S}(F=1)$	2 922 742 936 711	17

CIFODS. The corrections and uncertainties are summarized in Table I. By far the largest systematic shift which must be taken into account for such a measurement is due to the second-order Doppler effect. We determine this correction and estimate its uncertainty by varying model input parameters such as atomic velocity distribution, atomic beam/detector geometry, and laser pulse duration within limits given by the experimental restrictions.

The pressure shift, which includes collisions of hydrogen atoms with each other and with background gas, was the second-largest systematic shift in this measurement. The shift from hydrogen/hydrogen collisions can be calculated from the measured flux of atomic hydrogen using a molecular gas flow model and the known van der Waals potential [23]. For our flux (around 1.1×10^{18} atoms/s) the correction is +8.3(6.2) kHz; the uncertainty in this correction is set by the uncertainty of the distance between the nozzle and pulse collision volume, as well as the estimated value of the dissociation rate in our discharge. Collisions with background gas depend on the pressure of hydrogen in our apparatus, which was about 10^{-4} mbar. The correction calculated from the pressure of background gas is +2(1) kHz.

The dc Stark effect was potentially problematic because the measurement is made close to the lenses of the detector which are susceptible to patch charges. To mitigate this effect, the lenses were coated with carbon nanotubes, which provided a transparent and electrically conductive coating. Also, we surrounded the interaction volume with electrodes as shown in Fig. 3 and we zeroed the electric field by observing the line shifts and varying the voltage on three of the electrodes. The magnetic field was compensated to 20 mG using coils external to the vacuum chamber to suppress Zeeman shifts. Since the Landé g factors are the same for both the $1S$ and $3S$ states, there is no first-order shift. The 5-Hz uncertainty shown in Table I is due to the quadratic Zeeman shift which arises from mixing of the hyperfine levels.

The line-pulling systematic listed in Table I is caused by two effects—quantum interference due to off-resonant fine-structure components (also referred to as cross-damping) and the pulling from off-resonant laser comb modes. In a recent paper, we provide a detailed discussion of cross-damping and how it relates to this experiment [22]. This effect will cause the nearby $3D$ lines to distort our line shape in a way which depends on our laser excitation and detector geometry. The second effect taken into account, pulling from off-resonant comb modes, is largely canceled because there is a near symmetric set of off-resonant comb components on either side of the measured transition. Both effects are taken into account in the simulations and contribute to the listed uncertainty.

Including all systematic shifts and uncertainties, we arrive at a value for the $1S$-$3S$ $F=1$ to $F=1$ transition of 2 922 742 936 711(17) kHz, which is in excellent agreement with, but slightly less accurate than, the previous measurement using a cw laser [7]. Taking into account the hyperfine splitting of the $1S$ and $3S$ states [24,25], we come to a value for the $1S$-$3S$ centroid frequency of 2 922 743 278 659(17) kHz. While this measurement is limited by residual Doppler shifts, it was performed with a room temperature atomic beam. By simply cooling the beam to cryogenic temperatures, we should greatly mitigate systematic shifts arising from the velocity of the atoms. As mentioned earlier, our small detector size was an advantage for our study of the CIFODS. In the future a larger detector and more even sampling of the atomic trajectories would be preferable and allow us to use Eqs. (6) and (8) to estimate the size of the effect. Also, detailed studies of the source of the pulse chirp and methods to reduce and control this parameter are currently underway.

ACKNOWLEDGMENTS

D.Y. acknowledges support from the Alexander von Humboldt Foundation, R.P. from the European Research Council under Grant No. StG 279765, K.K. and N.K. from DFG Grant No. HA 1457/101-1 and RFBR Grant No. 14-0291331, and T.W.H. from the Max Planck Foundation. The authors acknowledge the Garching Rechnungszentrum for computation time.

[1] P. J. Mohr, B. N. Taylor, and D. B. Newell, Rev. Mod. Phys. **84**, 1527 (2012).
[2] R. Pohl *et al.*, Nature (London) **466**, 213 (2010).
[3] A. Antognini *et al.*, Science **339**, 417 (2013).
[4] R. Pohl, R. Gilman, G. A. Miller, and K. Pachucki, Annu. Rev. Nucl. Part. Sci. **63**, 175 (2013).
[5] C. G. Parthey, A. Matveev, J. Alnis, B. Bernhardt, A. Beyer, R. Holzwarth, A. Maistrou, R. Pohl, K. Predehl, Th. Udem, T. Wilken, N. Kolachevsky, M. Abgrall, D. Rovera, C. Salomon, P. Laurent, and T. W. Hänsch, Phys. Rev. Lett. **107**, 203001 (2011).
[6] C. Schwob, L. Jozefowski, B. de Beauvoir, L. Hilico, F. Nez, L. Julien, F. Biraben, O. Acef, J.-J. Zondy, and A. Clairon, Phys. Rev. Lett. **82**, 4960 (1999).
[7] O. Arnoult, F. Nez, L. Julien, and F. Biraben, Eur. Phys. J. D **60**, 243 (2010).
[8] E. Peters, D. C. Yost, A. Matveev, T. W. Hänsch, and T. Udem, Ann. Phys. (Berlin, Ger.) **525**, L29 (2013).

[9] S. Galtier, H. Fleurbaey, S. Thomas, L. Julien, F. Biraben, and F. Nez, J. Phys. Chem. Ref. Data **44**, 031201 (2015).
[10] Th. Udem, R. Holzwarth, and T. W. Hänsch, Nature (London) **416**, 233 (2002).
[11] A. Marian, M. Stowe, J. Lawall, D. Felinto, and J. Ye, Science **306**, 2063 (2004).
[12] S. Witte, R. T. Zinkstok, W. Ubachs, W. Hogervorst, and K. S. E. Eikema, Science **307**, 400 (2005).
[13] M. Herrmann, M. Haas, U. D. Jentschura, F. Kottmann, D. Leibfried, G. Saathoff, C. Gohle, A. Ozawa, V. Batteiger, S. Knünz, N. Kolachevsky, H. A. Schüssler, T. W. Hänsch, and Th. Udem, Phys. Rev. A **79**, 052505 (2009).
[14] C. Benko, T. K. Allison, A. Cingöz, L. Hua, F. Labaye, D. C. Yost, and J. Ye, Nat. Photonics **8**, 530 (2014).
[15] S. Galtier, F. Nez, L. Julien, and F. Biraben, Opt. Commun. **324**, 34 (2014).
[16] S. Reinhardt, E. Peters, T. W. Hänsch, and Th. Udem, Phys. Rev. A **81**, 033427 (2010).
[17] A. Ozawa and Y. Kobayashi, Phys. Rev. A **86**, 022514 (2012).
[18] I. Barmes, S. Witte, and K. S. E. Eikema, Phys. Rev. Lett. **111**, 023007 (2013).
[19] M. Haas, U. D. Jentschura, C. H. Keitel, N. Kolachevsky, M. Herrmann, P. Fendel, M. Fischer, Th. Udem, R. Holzwarth, T. W. Hänsch, M. O. Scully, and G. S. Agarwal, Phys. Rev. A **73**, 052501 (2006).
[20] G. Grynberg, F. Biraben, E. Giacobino, and B. Cagnac, J. Phys. (Paris) **38**, 629 (1977).
[21] H. A. Bethe and E. E. Salpeter, *Quantum Mechanics of One and Two-Electron Atoms* (Dover, New York, 2008).
[22] D. C. Yost, A. Matveev, E. Peters, A. Beyer, T. W. Hänsch, and Th. Udem, Phys. Rev. A **90**, 012512 (2014).
[23] L. A. Vainshtein, I. I. Sobelman, and E. A. Yukov, *Excitation of Atoms and Broadening of Spectral Lines* (Nauka, Moscow, 1979).
[24] S. G. Karshenboim, Phys. Rep. **422**, 1 (2005).
[25] U. D. Jentschura and V. A. Yerokhin, Phys. Rev. A **73**, 062503 (2006).